Journal of Materials Chemistry B

Accepted Manuscript

ROYAL SOCIETY OF CHEMISTRY

www.rsc.org/materialsB

Journal Name

RSCPublishing

ARTICLE

Reduced graphene oxide gated mesoporous silica nanoparticles as a versatile chemo-photothermal therapy system through pH controllable release

Cite this: DOI: 10.1039/x0xx00000x

Received 00th January 2012,
Accepted 00th January 2012

DOI: 10.1039/x0xx00000x

www.rsc.org/

Ting Ting Wang, [a] Jing Lan, [a] Yue Zhang, [a] Zhu Lian Wu, [b] Chun Mei Li, [a] Jian Wang [a] and Cheng Zhi Huang* [a b]

The synergistic therapy has become a potential treatment in the battles against diseases. In this work, we developed a novel versatile folate targeted system for cancer cells with the combination of chemotherapy and phototherapy by using mesoporous silica nanoparticles (MSNs) as a drug loading carrier, in which reduced graphene oxide (rGO) gated on MSNs by pH responsive detach. That is, rGO herein acts not only for gating control of the drug release but also for near-infrared photothermal therapy. With the drug loading system, photothermal conversion efficiency and excellent doxorubicin (DOX) loading capacity have been achieved, making the DOX loaded MSN@rGO-FA (DOX@MSN@rGO-FA) nanocomposites can kill 68% of HEp-2 cells in synergistic therapy, as compared with that 54% in photothermal therapy and 33% in chemotherapy, respectively, illustrating that the synergistic therapy strategy by present newly developed versatile drug loading system much more efficient as evaluated in vitro.

1. Introduction

Multifunctional mesoporous silica nanoparticles (MSNs) have been widely used as drug carrier due to their high colloidal stability, uniform and tunable pore size, large loading capacity, biocompatibility and easy surface modification.[1-3] For further making the MSNs drug carrier much more functional, general modifications have been adopted such as suitable gatekeepers, targeting groups, capping nanomaterials etc.[4, 5] The interesting gate keeping strategy by using proteins,[6, 7] DNA,[8, 9] polymers[10, 11] and nanoparticles[12, 13] to block the pore entrances of MSNs and the gatekeeper can be either opened or removed by appropriate stimulations such as pH,[14, 15] temperature,[16, 17] redox potential,[18, 19] etc. Furthermore, the gate keeping strategy can realize a synergistic effect for killing cancer cells combining chemotherapy of the drug and the therapeutic effect of gate keeper. [20] It is easy to realize the chemotherapy of the drug, while for the therapeutic effect of gate keeper, it has still be explored and has shown high promise to enhance the therapeutic efficacy.

Synergistic therapies are attracting more and more attentions in recent years, particularly in the research fields of cancer treatments. For example, photothermal therapy (PTT), a mild heating such as to about 42-43 ^{o}C, is frequently employed as an adjunctive method such as in chemotherapy, photodynamic therapy (PDT) and radiotherapy.[21] In principle, photothermal conversion agents were taken up by cells to generate heat from optical energy, leading to photo ablation of the cancer cells and subsequently cell death. For that purpose of PTT, a large number of the near-infrared (NIR) photothermal conversion agents, such as gold nanocages,[16] nanorods,[17] nanoroses,[22] copper chalcogenides,[23] carbon nanomaterials,[24] have been intensively reported.

As a shining star in the nanomaterials science, graphene oxide (GO) has been exploited as nano-carriers for gene or drug delivery for cancer therapy.[25, 26] Various nanoparticles have been grown on GO surfaces or GO have been reduced in order to improve optical properties of GO. Particularly, some groups have demonstrated that rGO presented dramatically enhanced NIR absorption compared to that of GO.[27-29] In terms of the excellent properties of rGO, developing rGO as heating gatekeeper coat on MSNs and making their synergistic ablation for tumor cells in vitro through the combination of chemotherapy and photothermal therapy seem to be interesting.

In such case, herein we designed and prepared a multifunctional drug delivery system based on the rGO and MSNs. The cargo molecules could be released in acidic environment due to the well-known pH dependence of cleavage of the C=N bonds of the Schiff' base –bond (the action step can be seen in Electronic Supplementary Information eq.3 and 4).[30, 31] As depicted in Scheme 1, at first, amino-modified mesoporous silica nanoparticles loading DOX (DOX@MSN-NH_2) were synthesized, and then cross-linked by glutaraldehyde (GA) and branched polyethyleneimine (PEI) to form C=N bonds (the form of C=N bonds can be seen in Electronic Supplementary Information eq.1 and 2), leading to the nanoparticles surface with positive charge. As a result, the as-prepared MSN-PEI can be encapsulated by negatively charged rGO *via* electrostatic

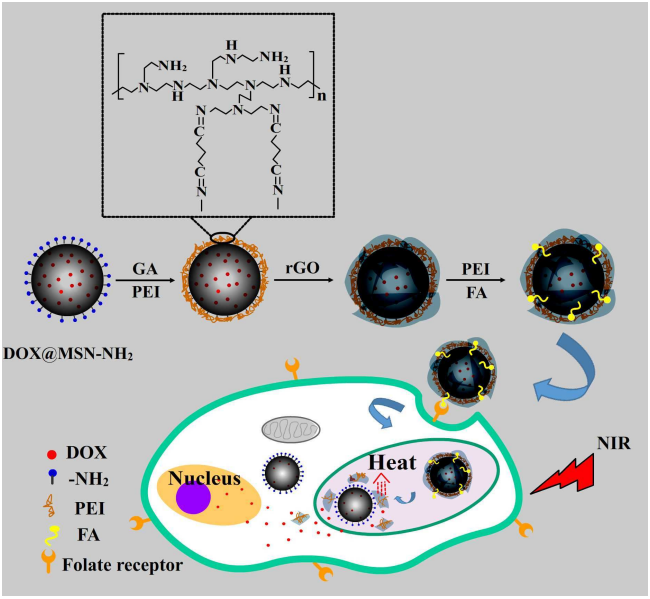

Scheme 1. Schematic illustration of the preparation process of folate targeted anticancer drug delivery system (DOX@MSN@rGO-FA) and synergistic therapy combination of chemotherapy and phototherapy for cancer cells in *vitro*.

interaction. Finally, folic acid (FA) molecules were attached to the nanocomposites for targeting specific cells with FA receptors. With the entrance of the multifunctional nanoparticles into the cancer cells, the low pH in cellular endosomes can lead to the detachment of rGO which attaching with PEI from MSN because of cleavage of the C=N bonds and the release of DOX to kill the cells. As the results, the rGO can burn cells under NIR irradiation.

2. Materials and methods

2.1. Materials

Tetraethylorthosilicate (TEOS, 99%) was purchased from Fluka. Cetyltrimethylammonium bromide (CTAB) was obtained from Sinopharm Chemical Reagent Co. Ltd (Shanghai, China). Doxorubicin hydrochloride (DOX•HCl, 98%) was purchased from Dalian Meloney Biotechnology Co. Ltd (Dalian, China). (3-Aminopropyl) trimethoxysilane (APTES), glutaraldehyde (GA, 50% in water), branched polyethyleneimine (PEI, Mw=70,000) were gained from Alfa Aesar. Graphene oxide was purchased from Nanjing XFNano Material Tech Co., Ltd. 5 and 6-carboxy fluorescein diacetate succinimidyl esters (CFSE) were obtained from Dojindo Laboratories. All Other reagents were of analytical grade. Millipore water with 18.2 MΩ was used in the experiment.

2.2. Synthesis of reduced graphene oxide (rGO)

GO suspension was sonicated about 2 h until it becomes into a clear solution, and 0.25 mg/mL GO then was mixed with 25 mg gallic acid in 50 mL of aqueous solution in a flask. After adjusting the pH of the mixture to 9 with 0.2 mol/mL NaOH solution, the flask was put into a water bath at 90 ^{o}C for 1 h. The uniformly dispersed black solution of rGO was then filtered and washed with water to remove excess gallic acid and NaOH, and the resulting solid was dried and then resuspended in water.

2.3. Synthesis of amino-modified mesoporous silica nanoparticles (MSN-NH_2)

MSN-NH_2 nanoparticles were synthesized according to the literature.[32] Briefly, cetyltrimethylammonium bromide (CTAB, 250 mg) and Pluronic F127 ($EO_{70}PO_{106}$ EO_{70}, 25 mg) were dissolved in deionized H_2O (120 mL), followed by the addition of 0.875 mL NaOH solution (aq, 2 M) and heated the solution to 80 ^{o}C. TEOS (1.25 mL) was added dropwise to the surfactant solution. After stirring for 2 h at 80 ^{o}C, blue white colloidal solution resulted. Centrifugation and washing with deionized water and methanol, the resulting solids were then dried at room temperature under vacuum. In order to remove the surfactant from the nanopores of the nanoparticles, 300 mg as-made MSN-CTAB was suspended in a mixture of MeOH (36 mL) and HCl (2 mL) solution. The solution was heated twice under reflux for 12 h, and then extensively washed with $NaHCO_3$ solution, deionized water and MeOH. The resulting product was placed under vacuum to remove the remaining solvent in the mesopores. MSNs (200 mg) were dispersed in anhydrous ethanol (40 mL), then heated to 80 ^{o}C. APTES (2 mL) was added into the solution to graft MSNs with amino groups. The reaction mixture was refluxed for 24 h, and followed by centrifugation, washed with ethanol for three times and dried.

2.4. Loading of doxorubicin to MSN-NH_2

MSN-NH_2 (20 mg) was dispersed in deionized water solution (16 mL), followed by adding DOX (10 mg) and stirring in the dark for 24 h at room temperature. The resulting material was centrifuged and washed thoroughly with deionized water and dried under vacuum (DOX@MSN-NH_2). All supernatants were collected together. The amount of loaded DOX for MSN-NH_2 was analyzed by a UV-vis spectrophotometer at 481 nm and calculated as below.
Loading efficiency (LE%) = (weight of loaded DOX)/ (initial weight of DOX).
Loading content (LC%) = (weight of loaded DOX/weight of DOX carrier).

2.5. Crosslinking of MSN-NH_2(or DOX@MSN-NH_2) and PEI by glutaraldehyde

MSN-NH_2 (or DOX@MSN-NH_2, 30 mg) was suspended in 1% GA aqueous solution (4 mL). The suspension was stirred at room temperature for 24 h followed by centrifugation. The precipitate was then washed extensively with deionized water to remove GA and dried under vacuum to obtain GA-activated mesoporous silica nanoparticles. MSN-GA (or DOX@MSN-GA, 20 mg) was stirred in deionized water solution (35 mL) containing PEI (1.0 mg/mL, Mw = 70,000) for 24 h at room temperature. Branched PEI functioned silica particles (MSN-PEI or DOX@MSN-PEI) were washed several times with deionized water by centrifugation to remove physically adsorbed PEI and dried.

2.6. Preparation of rGO gated MSN-PEI or DOX@MSN-PEI

MSN-PEI (or DOX@MSN-PEI) nanoparticles (20 mg) were suspended in water by bath sonication and rGO suspension (5 mL,

1.0 mg/mL) was added later, then mixture was stirred at room temperature for 24 h to complete the electrostatic wrapping process. The MSN@rGO (or DOX@MSN@rGO) product was then collected by centrifugation at 12000 rpm and thoroughly washed with water to remove any suspended rGO residues and dried.

2.7. Folate conjugation on MSN@rGO (or DOX@MSN@rGO) nanoparticles

In order to conjugate FA on MSN@rGO (or DOX@MSN@rGO) nanoparticles, we introduced amino on the rGO by PEI. MSN@rGO (or DOX@MSN@rGO) nanoparticles (20 mg) were suspended in PEI aqueous solution (20 mL, 1.0 mg/mL) and stirred at room temperature for 24 h. The MSN@rGO-NH_2 (or DOX@MSN@rGO-NH_2) was obtained by centrifugation and drying. FA was then conjugated with MSN@rGO-NH_2 (or DOX@MSN@rGO-NH_2) by reaction between the NH_2 groups of the MSN@rGO-NH_2 (or DOX@MSN@rGO-NH_2) and COOH groups on the FA molecules.[33] Briefly, FA (16 mg) was activated by 1-ethyl-3-(3-dimethylaminopropyl)carbodiimide hydrochloride (EDC, 8 mg) and N-hydroxysuccinimide (NHS, 4.8 mg) which were dissolved in DMSO solution (5 mL) and the mixture was stirred for 24 h. 20 mg of MSN@rGO-NH_2 (or DOX@MSN@rGO-NH_2) nanoparticles were added to the activated FA solution and reacted with stirring for 24 h at room temperature. Then, the mixture was centrifuged and washed with deionized water and ethanol three times, respectively. The products were dried under vacuum and obtained MSN@rGO-FA (or DOX@MSN@rGO-FA).

2.8. In *vitro* drug release

In a typical release experiment, 4 mg of DOX@MSN-NH_2 or DOX@MSN@rGO nanocomoposites were dispersed in Phosphate buffered saline (PBS, pH 7.4 or 5.0). The dispersion was then transferred into a dialysis bag (cut off molecular weight: 8,000-14,000 kDa), which was subsequently placed into a 100 mL buffer solution at 37 ^oC and shaken at 150 rpm. At desired time intervals, 1.0 mL of the release media of DOX@MSN-NH_2 or DOX@MSN@rGO nanocomoposites (without NIR) was withdrawn from the solution and replenished with an equal volume of fresh medium. For the DOX@MSN@rGO nanocomoposites with NIR, at predetermined time intervals, the samples were irradiated with NIR laser at 980 nm for 15 min and release media withdraw before and after NIR laser irradiation. The released DOX was analyzed by UV-vis spectroscopy.

2.9. Measurements of photothermal effect

To investigate the photothermal heating effect, MSN@rGO nanocarriers with a series of concentrations (100, 200, and 500 μg/mL) were prepared. A volume of 100 μL solution was placed in a 96-well plate and then irradiated with a NIR laser (wavelength, 980 nm; power, 1.25W; laser spot diameter, 3 mm) at same time intervals (1 min). Solution temperature was monitored by a digital thermometer immediately after irradiation. The control experiment of negative sample (H_2O) was also measured under the same conditions.

2.10. Cell uptake

To check cellular uptake of nanoparticles, HEp-2 cells and A549 cells were seeded onto 8 mm square glass coverslips placed in 24-well plates at a density of 5×10^4/well and cultured for 24 h. HEp-2 cells were treated with free DOX·HCl, DOX@MSN@rGO and DOX@MSN@rGO-FA for 3 h (DOX · HCl concentration = 5 μg/mL). Among them, the cells treated with DOX@MSN@rGO-FA including cells pre-treated with 50 μg/mL free FA and those without treatment. A549 cells were treated with DOX@MSN@rGO-FA for 3 h. Then, the cells were washed and fixed with 4% formaldehyde for 30 min. Fluorescence images were taken by confocal laser scanning microscopy (CLSM).

2.11. In *vitro* cell toxicity assay

The cytotoxicity was quantified by a CCK-8 assay using HEp-2 cells. HEp-2 cells were seeded in a 96-well plate at 1×10^4/well in 100 μL medium, after being incubated at 37 °C and 5% CO_2 for 24 h. A series of MSNs, MSN@rGO, DOX@MSN@rGO and DOX@MSN@rGO-FA nanoparticles with different concentrations were added. After incubating for 48 h, the cell viability was determined by cell-counting kit-8 (CCK-8) assay.

2.12. In *vitro* photothermal and chemo-phothermal assay

HEp-2 cells were plated in a 96-well plate at 1×10^4/well in 100 μL medium. After 24 h, MSN@rGO-FA and DOX@MSN@rGO-FA nanocomoposites (suspended in medium) at the indicated concentrations were added. After incubation for 12 h, excess unbound nanoparticles were removed by rinsing three times with PBS. Fresh culture medium was then added to the wells. The cells were exposed to NIR light (wavelength, 980 nm; power, 1.25 W; laser spot diameter, 3 mm) for 15 min for photothermal and chemo-phothermal treatments, and then incubated again at 37 ^oC with 5% CO_2 for 36 h. After treatment, the cell viability was determined by CCK-8 assay.

2.13. Confocal fluorescence imaging analysis

HEp-2 cells were plated at a density of 4.0×10^5 cells per dishes on glass bottom cell culture dishes for 24 h. MSN@rGO-FA (100 μg/mL) and DOX@MSN@rGO-FA nanoparticles (the concentration of DOX was 20 μg/mL) were added and incubated for 12 h. After incubation for 12 h, the culture medium with nanoparticles was removed and the cells were resupplied with fresh culture medium. For thermal therapy, corresponding culture dishes were irradiated with a 980 nm NIR laser (power, 1.25W; laser spot diameter, 3 mm) for 15 min. After laser irradiation, the cells were then incubated again at 37 ^oC with 5% CO_2 for 36 h. After incubation was completed, the cells were then washed three times with PBS and stained in green with 20 μM of carboxy-fluorescein succinimidyl ester (CFSE).

2.14. Characterization

High resolution-transmission electron microscopic (HR-TEM) images were taken with a JEM-2100 microscope operating at 200 kV. Atomic force microscopic (AFM) images were measured by a Dimension Icon Scan Asyst atomic force microscope (Bruker Co.) Powder X-ray diffraction (XRD) analysis was obtained from an XD-3 X-Ray diffractometer using Cu (36 kV, 20 mA) radiation. The

absorption spectra were carried with a UV-3600 UV-vis-NIR spectrophotometer (Shimadzu, Japan). The surface area was calculated by the Brunauer-Emmett-Teller (BET). The pore size distribution was determined by the Barrett-Joyner-Halenda (BJH) method. The cells were imaged using an Olympus IX81LCS-DSU Disk Scanning confocal microscope (Olympus, Japan). Fourier transform infrared (FT-IR) spectra were recorded on an IRPRESTIGE-21 spectrometer (Shimadzu). Thermal gravimetric analyses (TGA) were performed using a SDT-Q600, USA. Zeta potential measurement was performed using a Zetasizer Nano-ZS90 instrument (Malvern Inc).

3. Results and discussion

3.1. Preparation and characterization of MSN and MSN@rGO

AFM was used to study the morphological characteristics of rGO. From the AFM image (Fig. 1A), the thickness of rGO remain unaltered at 1.2 nm, which suggests a single or two layered sheets.[34] TEM image of the rGO shows that part of the rGO layer structure below 100 nm (Fig. S1A). The average size of rGO is around 110 nm that can been seen from DLS spectra (Fig. S1B). Fig. 1B shows the typical FTIR spectra of GO and rGO. There are two peaks at 1728 cm^{-1} (C=O stretching vibrations from carbonyl) and 1068 cm^{-1} (C-O stretching vibrations) in the GO sample which testify the presence of many oxygen-containing functional groups. In comparison with the FTIR spectrum of GO, the peaks at 1728 cm^{-1} and 1068 cm^{-1} of rGO almost disappear. This is because the C-O-C, C=O and O-C=O are partly removed by gallic acid. TEM image shows that the average diameter of MSNs is about 145 nm (Fig. 1C). In Fig. 1D, the selected area electron diffraction (SAED) patterns obtained from rGO sheets attached to (but slightly removed from)

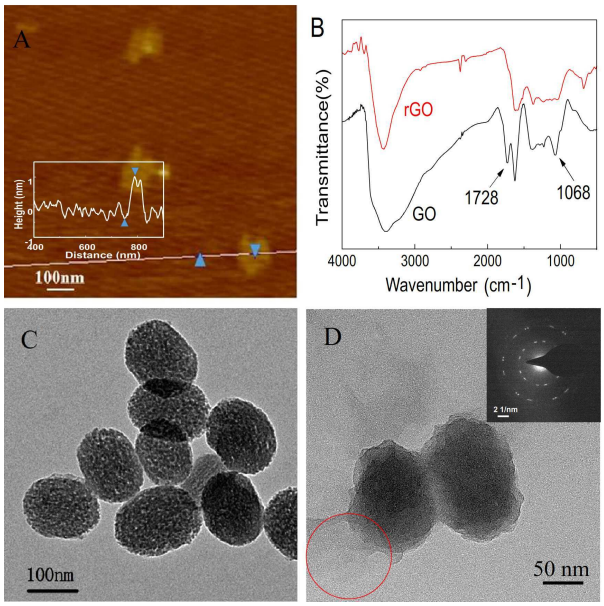

Fig. 1. Characterization of the as-prepared rGO, MSNs and MSN@rGO. (A) AFM image and AFM height analysis of rGO. (B) FTIR spectra of GO and rGO. (C, D) TEM images of the as-prepared MSN(C), MSN@rGO (D) and SAED pattern from the rGO is shown in the inset.

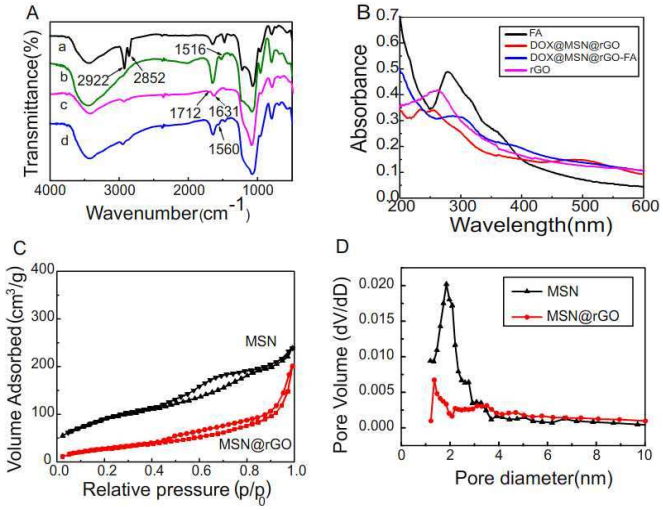

Fig. 2. (A) FTIR spectra of MSN-CTAB (a), MSN-NH_2 (b), MSN-GA (c) and MSN-PEI (d). (B) UV/vis spectra of FA (*c*, 25 μg/mL), rGO (*c*, 5 μg/mL), DOX@MSN@rGO (*c*, 100 μg/mL) and DOX@MSN@rGO-FA (*c*, 100 μg/mL). (C) Nitrogen adsorption-desorption isotherms for the as-synthesized MSNs and MSN@rGO. (D) The pore size distributions of the MSNs and MSN@rGO.

the MSNs shows a crystalline structure, [35] which demonstrates the rGO sheets act as gatekeeper on the MSNs. In Fig. S2A of TEM image, channel structure of MSN-PEI nanoparticles become blurred but no distinct lamellar structure on it in SEM image (Fig. S2B). Fig. S2C shows that rGO adhere to the MSN-PEI. XRD characterization for the structure of MSNs exhibits the mesoporous characteristic low-angle reflecting of a hexagonal-ordered array indexed as (100), (110) and (200) Bragg peaks (Fig. S3).[36, 37]

FTIR was used to confirm the successful functionalization of MSNs. As seen in Fig. 2A, the peak around 1092 cm^{-1} is due to asymmetric stretching of Si-O-Si bond in the silica nanoparticles. The surfactant removal process is testified by the disappearance of peaks at 2852 and 2922 cm^{-1}, which are attributed to the large amount of CTAB. [18, 38] After refluxing and reacting with APTES, a new peak assigns to N-H asymmetric bending at 1516 cm^{-1} appear, confirming the successful functionalization of MSNs with amino groups.[32] The spectrum of the GA-activated silica exhibits a new absorption band of the carbonyl groups (C=O) at about 1712 cm^{-1} and the stretching vibration of C=N at 1631 cm^{-1}.[39] The absorption band of the GA carbonyl groups disappeared. Additionally, the N-H bending vibration is detected at 1560 cm^{-1}, along with the C-N stretching vibration at 1472 cm^{-1} demonstrating that PEI has been linked with the GA-activated silica.

The rGO coating on DOX@MSN-PEI and the conjugation of folic acid on DOX@MSN@rGO nanoparticles can be identified by measuring UV/vis absorption. Fig. 2B shows the main characteristic absorption peak of rGO at 260 nm is found in the spectrum of DOX@MSN@rGO nanoparticles, which indicates that rGO has been successfully coated on the nanoparticles. It can be observed that the peak of FA is found at 288 nm on the spectrum of DOX@MSN@rGO-FA nanoparticles, which suggests that FA ligands have been grafted by amide reaction. The FTIR technique further demonstrates that FA ligands have been successfully

functioned onto MSN@rGO nanoparticles (Fig. S4). However, a bathochromic shift can be noted compared to the FA, which reveals the modification in the environment of the FA between the free and grafted states.[40] Zeta potential of the resultant nanoparticles was determined after each modification step (Fig. S5). MSN-NH_2 exhibits a positive potential of +19.6 mV due to the amine groups on the surface. After conjugation of PEI, the obtained nanoparticles still shows a positive potential suggesting that -NH_2 of PEI graft on the surface of nanoparticles. The rGO sheets show a negative charge over the surface. Thus, the formation of MSN@rGO with a negative potential of -35.1 mV was due to the strong electrostatic interaction between the positively charged MSN-PEI and negatively charged rGO sheets.

The N_2 adsorption-desorption isotherm and pore-size distribution curves of the as prepared MSNs and MSN@rGO nanoparticles are shown in Fig. 2C-D. The N_2 adsorption-desorption isotherm of MSNs can be classified as type-IV isotherm, suggesting that the MSN nanoparticles were mesoporous.[41, 42] The BET surface area is 308 m^2 g^{-1} and the pore volume is 0.37 cm^3 g^{-1}. Narrow pore diameter distribution (1.8 nm) is calculated by applying the BJH calculation to the adsorption isotherm. After capping the MSN-PEI with rGO, the surface area and pore volume significantly decrease to 109 m^2 g^{-1} and 0.31 cm^3 g^{-1} respectively. In addition, the pore diameter of MSN@rGO decreases to 1.4 nm. The change of sorption type together with the decrease of surface area and pore size distribution indicate the capping effect of the rGO. As shown in the thermal gravimetric analysis (TGA) curves in Fig. S6, when the temperature increase to 700 °C the weight loss of rGO at 400 °C due to the bulk pyrolysis of the carbon skeleton and MSN-PEI shows weight loss attribute to the burning of the organic functions. We also observed that MSN@rGO shows weight loss at 400 °C and it further makes it clear that the rGO is successfully grafted on the MSN.

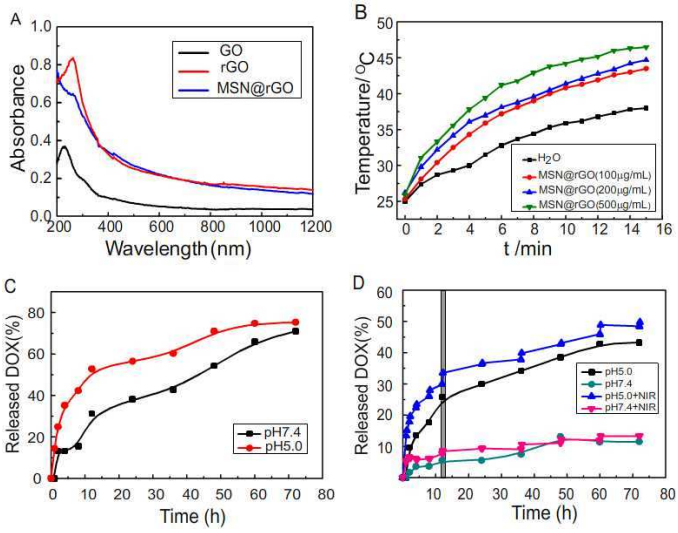

Fig. 3. (A) UV-vis-NIR absorbance spectra of GO, rGO (at the same concentration of 10 μg/mL) and MSN@rGO (the concentration was 100 μg/mL). (B) Photothermal heating curves of water and MSN@rGO solutions in different concentrations, all the solutions exposed to the 980nm laser (1.25 W) and the laser spot diameter was 3 mm. (C) Cumulative drug release from DOX@MSN systems in PBS of different pH values. (D) Cumulative drug release from DOX@MSN@rGO systems in PBS of different pH values with or without NIR for 15 min. Labelled part in figure represent NIR.

3.2. Photothermal effect of MSN@rGO

The rGO shows a significant ~ 4.0 folds increase in the NIR absorption at 980 nm (Fig. 3A), consistent with the higher light absorption in the visible and infrared region of reduced GO previously noted.[24] The increase was directly related to the degree of π conjugation in GO. GO was highly oxidized with disrupted π conjugation while chemical reduction restored part of the π conjugation.[28, 43] Once the rGO gated on MSN, the nanocomposites also exhibited dramatically enhanced NIR absorption of 3.6 folds at 980 nm compare to the GO.

MSN@rGO nanoparticles could convert NIR light energy into thermal energy, and thus we investigated the heat generation upon NIR irradiation for various solutions containing MSN@rGO and water only as control. As shown in Fig. 3B, the concentration dependent phothothermal heating effect (from 100 μg/mL to 500 μg/mL) is observed, and all the samples temperature reach to 43.5 °C within 15 min of irradiation. In contrast, under the same laser irradiation condition, the water remains about 38 °C.

3.3. Drug loading and release

To investigate the pH-responsive gating behavior of the nanomaterials, DOX was first loaded. DOX@MSN-PEI have been characterized by TGA (Fig. S6) and it was found that the weight loss increased by 20.9 wt% compared with MSN-PEI, suggesting the drug loading content is 20.9 wt%. The release profiles of DOX@MSN-NH_2 are measured at pH values of 7.4 and 5.0 at 37 °C for 72 h. As can be seen in Fig. 3C, DOX release fast at pH 5.0 than pH 7.4 in 12 h and cumulative release amount between different pH values in 72 h is equal. However, in Fig. 3D, no more than 11.5% of DOX is released from DOX@MSN@rGO at PBS pH 7.4 within 72 h, indicating an efficient capping of the rGO. At pH 5.0, the release amount reach to 42.3% after 72 h, which is almost 4.0 folds of that at pH 7.4. This difference in release rates should mainly be own to the pH dependence of cleavage of the C=N bonds of the Schiff's base bond. PEI separate from MSN along with the C=N bonds breaking in acid environment and rGO attaching with PEI via electrostatic interaction detach from MSN. Considering the fact that the tumor tissues are more acidic than the normal tissues,[44] the prepared DOX@MSN@rGO nanocarriers would be able to release the drug in the tumor tissues on demand with little premature release to minimize the side effects of DOX. We then explored the controlled release with NIR laser. DOX release under NIR laser is slightly higher than that without NIR at pH 5.0 and DOX release remain essentially unchanged with or without NIR laser at PBS pH 7.4, suggesting that DOX is temperature – dependent release.

3.4. Confocal laser scanning microscopy (CLSM) imaging

The uptake and intracellar distribution of the DOX@MSN@rGO-FA was investigated using confocal laser scanning microscopy (CLSM). Folate receptor positive (FR^+) cells HEp-2 and folate receptor negative (FR^-) cells A549 were chosen as the model cancer cells to verify the role of FA on cellular uptake of DOX@MSN@rGO-FA.[45, 46] Free DOX was

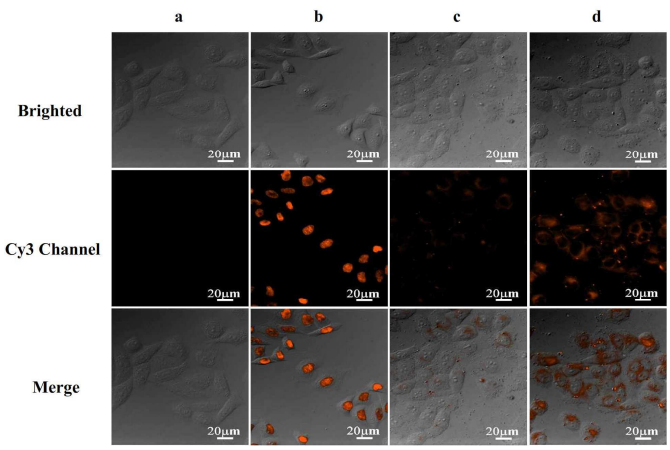

Fig. 4. Confocal fluorescence images of HEp-2 cells incubated with control (a), free DOX (b), DOX@MSN@rGO-FA with free FA (c) and DOX@MSN@rGO-FA (d) at a DOX concentration of 5 μg/mL for 3 h.

primarily accumulated in the cells by passive diffusion (Fig. 4b). To demonstrate that enhanced cellular internalization of DOX@MSN@rGO-FA nanocomposites is mediated *via* the folate receptor, a competition experiment was performed by pre-incubating with free folic acid. In Fig. 4c-d, the cells incubated with DOX@MSN@rGO-FA exhibit much stronger DOX fluorescence than those added of folate in the medium.

These results confirm that the cellular uptake of DOX@MSN@rGO-FA is associated with the FA receptor-mediated endocytosis of HEp-2 cells. Moreover, rather weak DOX fluorescence are observed for HEp-2 cells incubated with DOX@MSN@rGO without folate conjugation and for A549 cells incubated with DOX@MSN@rGO-FA (Fig. S7 and Fig. S8), which further corroborate that nanocomposites modified with FA facilitate recognition by HEp-2 cells and enhance the cellular uptake.

3.5. In *vitro* cytotoxicity and the photothermal and chemo-phothermal effect assay

As discussed above, the MSN@rGO nanocomposite is a synergistic platform for drug carrier and photothermal therapy. The ideal drug carriers and photothermal agents should have low-toxicity for biological applications. Cell viability for Hep-2 cells being incubated with MSNs and MSN@rGO nanocomposites of different concentrations for 24 h and 48 h was determined by CCK-8 assay. It is found that whether the MSNs or MSN@rGO nanocomposites exhibit no significant cytotoxicity, even at a high concentration of 100 μg/mL for 48 h (Fig. S9). Therefore, the nanomaterials were biocompatible. Based upon the cytotoxicity analysis, we limited the amount of MSN@rGO nanocomposites within 100 μg/mL in following cell studies.

To investigate the chemotherapy of DOX from nanoparticles, HEp-2 cells were incubated with the DOX@MSN@rGO and DOX@MSN@rGO-FA nanoparticles for 48 h at different DOX concentrations (from 0.1 μg/mL to 20 μg/mL) and then the CCK-8 assay was carried out to test the cell viability. Both DOX@MSN@rGO and DOX@MSN@rGO-FA nanoparticles show obvious cytotoxicity to HEp-2 cells and the inhibition ratio against HEp-2 cells increase with the increased of DOX concentration (Fig. 5A). The DOX@MSN@rGO-FA show higher cytotoxicity than the DOX@MSN@rGO under equivalent conditions, which further testify that the DOX@MSN@rGO-FA nanoparticles as anticancer drug delivery vehicles can be selectively taken up by targeted cancer cells.

We have also further illustrated whether the NIR laser radiation can improve the cell killing efficacy of the DOX@MSN@rGO-FA nanocomposites. Direct irradiation of the cells with laser in the absence of nanocomposites induced no appreciable negative effect on the viability of cells (Fig. 5B). However, the laser irradiation lead to significant decrease of the cell viability to 48% after the cells were incubated with 100 μg/mL of MSN@rGO-FA nanocomposites, suggesting that the heat generated from the NIR irradiation could efficiently kill cells. Without the NIR irradiation, 33.4% of the cells are killed

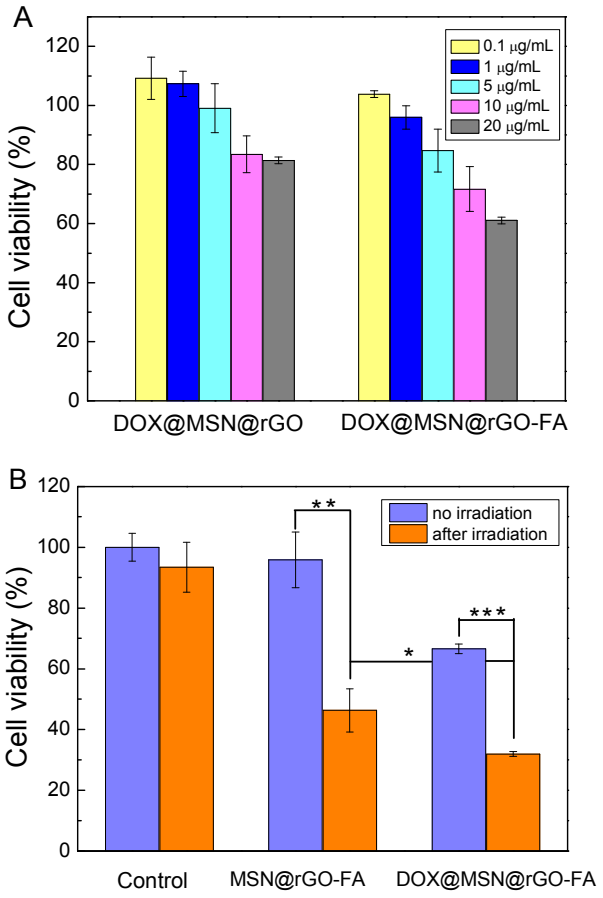

Fig. 5. Therapeutic effect evaluation of the nanocomposites by CCK-8 assays. (A) Cell viabilities of DOX@MSN@rGO and DOX@MSN@rGO-FA nanoparticles against HEp-2 cells at different DOX concentrations for 48 h (from 0.1 μg/mL to 20 μg/mL). (B) In vitro cytotoxicity of HEp-2 cells incubated with MSN@rGO-FA nanocomposites (100 μg/mL) and DOX@MSN@rGO-FA nanocomposites (100 μg/mL, the concentration of DOX was 20 μg/mL) with and without 980 nm NIR laser irradiation (power, 1.25W; laser spot, 3 mm) for 15 min. p values were calculated by the student's t test: * $p < 0.05$, ** $p < 0.01$, *** $p < 0.005$, $P < 0.05$ was considered to be statistically significant difference.

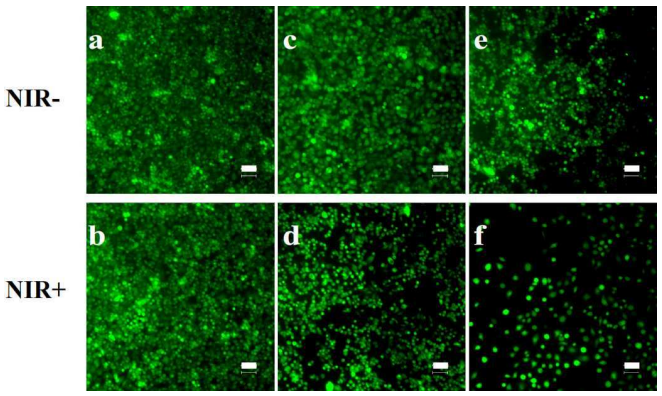

Fig. 6. CLSM images of HEp-2 cells incubated with: PBS (a, b), MSN@rGO-FA nanocomposites (c, d) and DOX@MSN@rGO-FA nanocomposites (e, f) in RPMI-1640 medium for 48 h at 37 °C, (top) without or (bottom) with NIR irradiation for 15 min at 980 nm (1.25W, laser spot, 3 mm). Scale bars are 40 μm.

by the DOX@MSN@rGO-FA nanocomposites, which should be attributed to the release of DOX from the nanocomposites.

In comparison, under the NIR irradiation, a higher cytotoxicity with 68.0% of cell death can be reached at an equivalent DOX concentration of 20 μg/mL. All the results demonstrate that the successful combination of chemotherapy and photothemal therapy in the DOX@MSN@rGO-FA nanocomposites can significantly improve the therapeutic efficacy. Therefore, DOX@MSN@rGO-FA nanocomposites could realize a synergistic effect for killing cancer cells through combining photothermal therapy and chemotherapy.

To further evaluate the therapeutic effect of DOX@MSN@rGO-FA nanocomposites, the live cells were stained by CFSE and imaged by a fluorescence microscope. As displayed in Fig. 6 a, b, c, no apparent change in cell viability is observed when cells were treated with a laser and MSN@rGO-FA nanocomposites alone compared with the negative control. And most of the cells are spindly and well maintain with favorable adherence that can be observed from the bright field microscope (Fig. S10a~c). However, cells treated with MSN@rGO-FA nanocomposites plus a 15 min NIR irradiation or with DOX@MSN@rGO-FA nanocomposites alone experience substantial cellular death (Fig. 6d, e). The density of cells decreased with obviously shrunken and deteriorative adherence (Fig. S10d~e). All the results suggested that MSN@rGO-FA could convert the NIR light into the heat to destruct cells and DOX@MSN@rGO-FA nanocomposites exhibit chemotherapy. Notably, after NIR laser irradiation to the HEp-2 cells incubated with DOX@MSN@rGO-FA nanoparticles, a significant decrease in cell viability and unhealthy appearance of cells was found (Fig. S10f). All the results show that DOX@MSN@rGO-FA nanocomposites exhibit a higher cell killing efficacy for HEp-2 cells than individual therapy due to enhanced toxicity of DOX and hyperthermia (Fig. 6f).

Conclusions

In summary, we have developed a multifunctional nanoplatform (DOX@MSN@rGO-FA nanocomposites), which can combine photothermal therapy and chemotherapy in a system. The unique advantages of such multifunctional nanoparticles include: 1) the DOX and photothermal agent can be specifically delivered into cancer cells via a receptor-mediated endocytosis pathway owing to FA target that can minimize nonspecific toxicity; 2) the rGO nanosheets as the gatekeeper can detach from the silica and expose the pores of mesoporous silica in the acidic environment reducing the release of DOX in normal cells; 3) the rGO can effectively absorb and convert NIR light to heat upon irradiation with NIR laser. When the multifunctional nanoplatform enters into cancer cells followed by NIR light irradiation, both chemotherapy and photothermal therapy can be activated. More importantly, this nanocomposite can achieve the synergistic chemo-photothermal therapy effect and shows better therapy effect than individual therapy. These results may raise possibilities of a potential nanoplatform using multifunctional nanocomposites for cancer therapy.

Acknowledgements

This work was supported by the National Natural Science Foundation of China (NSFC, 21035005), and the National Basic Research Program of China (973 Program, no. 2011CB933600).

Notes and references

[a] Key Laboratory of Luminescent and Real-Time Analytical Chemistry, Ministry of Education, College of Pharmaceutical Sciences, Southwest University, Chongqing 400715, China
[b] College of Chemistry and Chemical Engineering, Southwest University, Chongqing 400715, China

† Electronic Supplementary Information (ESI) available: [eq. 1, 2, 3 and 4, TEM image, DLS spectra, SEM images, XRD curve, FTIR spectra, ζ-potential, TGA curve, confocal fluorescence images, cell viabilities and bright field images of nanoparticles]. See DOI: 10.1039/b000000x/

1. S. Sreejith, X. Ma and Y. Zhao, J. Am. Chem. Soc., 2012, 134, 17346 – 17349.
2. J. Wang, T. T. Wang, P. F. Gao and C. Z. Huang, J. Mater. Chem. B, 2014, 2, 8452-8465.
3. J. Wang, P. P. Gao, X. X. Yang, T. T. Wang, J. Wang and C. Z. Huang, J. Mater. Chem. B, 2014, 2, 4379-4386.
4. C. Argyo, V. Weiss, C. Bräuchle and T. Bein, Chem. Mater., 2013, 26, 435-451.
5. C. Chen, F. Pu, Z. Huang, Z. Liu, J. Ren and X. Qu, Nucleic Acids Res, 2011, 39, 1638-1644.
6. A. Parodi, S. G. Haddix, N. Taghipour, S. Scaria, F. Taraballi, A. Cevenini, I. K. Yazdi, C. Corbo, R. Palomba, S. Z. Khaled, J. O. Martinez, B. S. Brown, L. Isenhart and E. Tasciotti, ACS Nano, 2014, 8, 9874–9883.
7. S. Wu, X. Huang and X. Du, Angew. Chem. Int. Ed., 2013, 52, 5580 – 5584.

8. P. Zhang, F. Cheng, R. Zhou, J. Cao, J. Li, C. Burda, Q. Min and J.-J. Zhu, Angew. Chem. Int. Ed., 2014, 53 2371 –2375.
9. C. Chen, J. Geng, F. Pu, X. Yang, J. Ren and X. Qu, Angew. Chem. Int. Ed., 2011, 50, 882 –886.
10. C.-L. Zhu, X.-Y. Song, W.-H. Zhou, H.-H. Yang, Y.-H. Wen and X.-R. Wang, J. Mater. Chem., 2009, 19, 7765–7770.
11. A. Baeza, E. Guisasol, A. Torres-Pardo, J. M. González-Calbet, G. J. Melen, M. Ramirez and M. Vallet-Regí, Adv. Funct. Mater., 2014, 24, 4625–4633.
12. J. L. Vivero-Escoto, I. I. Slowing, C.-W. Wu and V. S.-Y. Lin, J. Am. Chem. Soc. , 2009, 131 3462–3463.
13. L. Zhou, Z. Li, Z. Liu, J. Ren and X. Qu, Langmuir, 2013, 29, 6396-6403.
14. F. Muhammad, M. Guo, W. Qi, F. Sun, A. Wang, Y. Guo and G. Zhu, J. Am. Chem. Soc. , 2011, 133, 8778 – 8781.
15. H. Meng, M. Xue, T. Xia, Y.-L. Zhao, F. Tamanoi, J. F. Stoddart, J. I. Zink and A. E. Nel, J. Am. Chem. Soc. , 2010, 132, 12690–12697.
16. J. Yang, D. Shen, L. Zhou, W. Li, X. Li, C. Yao, R. Wang, A. M. El-Toni, F. Zhang and D. Zhao, Chem. Mater. , 2013, 25, 3030−3037.
17. N. Li, Z. Yu, W. Pan, Y. Han, T. Zhang and B. Tang, Adv. Funct. Mater. , 2013, 23, 2255–2262.
18. X. Ma, K. T. Nguyen, P. Borah, C. Y. Ang and Y. Zhao, Adv. Healthcare Mater. , 2012, 1, 690–697.
19. D. Xiao, H.-Z. Jia, J. Zhang, C.-W. Liu, R.-X. Zhuo and X.-Z. Zhang, Small, 2014, 10, 591-598.
20. X. Liu, F. Fu, K. Xu, R. Zou, J. Yang, Q. Wang, Qian Liu, Z. Xiao and J. Hu, J. Mater. Chem. B, 2014, 2, 5358-5367.
21. D. Chen, C. Wang, F. Jiang, Z. Liu, C. Shu and L.-J. Wan, J. Mater. Chem. B, 2014, 2, 4726-4732.
22. C. Li, T. Chen, I. Ocsoy, G. Zhu, E. Yasun, M. You, C. Wu, J. Zheng, E. Song, C. Z. Huang and W. Tan, Adv. Funct. Mater., 2014, 24, 1772-1780.
23. J. Bai, Y. Liu and X. Jiang, Biomaterials, 2014, 35, 5805-5813.
24. M. Acik, G. Lee, C. Mattevi, M. Chhowalla, K. Cho and Y. J. Chabal, Nat. Mater., 2010, 9, 840-846.
25. L. Feng, S. Zhang and Z. Liu, Nanoscale, 2011, 3, 1252–1257.
26. W. Miao, G. Shim, S. Lee, S. Lee, Y. S. Choe and Y.-K. Oh, Biomaterials, 2013, 34, 3402-3410.
27. H. Kim, D. Lee, J. Kim, T.-i. Kim and W. J. Kim, ACS Nano, 2013, 7, 6735–6746.
28. J. T. Robinson, S. M. Tabakman, Y. Liang, H. Wang, H. S. Casalongue, D. Vinh and H. Dai, J. Am. Chem. Soc. , 2011, 133, 6825 – 6831.
29. K. Yang, J. Wan, S. Zhang, B. Tian, Y. Zhang and Z. Liu, Biomaterials, 2012, 33, 2206-2214.
30. J. Wang, H. Liu, F. Leng, L. Zheng, J. Yang, W. Wang and C. Huang, Micropor. Mesopor. Mater., 2014, 186, 187-193.
31. E. H. Cordes and W. P. Jencks, J. Am. Chem. Soc., 1963, 85, 2843–2848.
32. L. Xing, H. Zheng, Y. Cao and S. Che, Adv. Mater., 2012, 24, 6433–6437.
33. P. F. Gao, L. L. Zheng, L. J. Liang, X. X. Yang, Y. F. Li and C. Z. Huang, J. Mater. Chem. B, 2013, 1, 3202–3208.
34. X. Li, X. Wang, L. Zhang, S. Lee and H. Dai, Science, 2008, 319, 1229–1232.
35. I. K. moon, J. Lee, R. s. Ruoff and H. Lee, Nat. Commun., 2010, 1, 73.
36. L. Mondragón, N. Mas, V. Ferragud, C. d. l. Torre, A. Agostini, R. Martíinez-Máñez, F. Sancenón, P. Amorós, E. Pérez-Payá and M. Orzáez, Chem. Eur. J. , 2014, 20, 5271 – 5281.
37. X. Huang, N. Hauptmann, D. Appelhans, P. Formanek, S. Frank, S. Kaskel, A. Temme and B. Voit, Small, 2012, 8, 3579–3583.
38. L. Yuan, Q. Tang, D. Yang, J. Z. Zhang, F. Zhang and J. Hu, J. Phys. Chem. C, 2011, 115, 9926–9932.
39. S. He, W. Zhang, D. Li, P. Li, Y. Zhu, M. Ao, J. Li and Y. Cao, J. Mater. Chem. B, 2013, 1, 1270–1278.
40. Y. Zhu, Y. Fang and S. Kaske, J. Phys. Chem. C, 2010, 114, 16382–16388.
41. Y. Li, J. Wei, W. Luo, C. Wang, W. Li, S. Feng, Q. Yue, M. Wang, A. A. Elzatahry, Y. Deng and D. Zhao, Chem. Mater. , 2014, 26, 2438-2444.
42. J. E. Lee, N. Lee, H. Kim, J. Kim, S. H. Cho, J. H. Kim, T. Kim, I. C. Song, S. P. Park, W. K. Moon and T. Hyeon, J. Am. Chem. Soc. , 2010, 132, 552–557.
43. J. Kim, F. Kim and J. Huang, Mater. Today, 2010, 13, 28–38.
44. Y. Tang, Z. Teng, Y. Liu, Y. Tian, J. Sun, S. Wang, C. Wang, J. Wang and G. Lu, J. Mater. Chem. B, 2014, 2, 4356-4362.
45. S. Setua, D. Menon, A. Asok, S. Nair and M. Koyakutty, Biomaterials, 2010, 31, 714–729.
46. H. Wang, C. Liu, X. Gong, D. Hu, R. Lin, Z. Sheng, C. Zheng, M. Yan, J. Chen, L. Cai and L. Song, Nanoscale, 2014, 6, 14270-14279.

Graphic abstract

for

Reduced graphene oxide gated mesoporous silica nanoparticles as a versatile chemo-photothermal therapy system through pH controllable release

Ting Ting Wang, [a] Jing Lan, [a] Yue Zhang, [a] Zhu Lian Wu, [b] Chun Mei Li, [a] Jian Wang [a] and Cheng Zhi Huang* [a b]

a Key Laboratory of Luminescent and Real-Time Analytical Chemistry, Ministry of Education, College of Pharmaceutical Sciences, Southwest University, Chongqing 400715, China
b College of Chemistry and Chemical Engineering, Southwest University, Chongqing 400715, China
* Corresponding Author. E-mail: chengzhi@swu.edu.cn

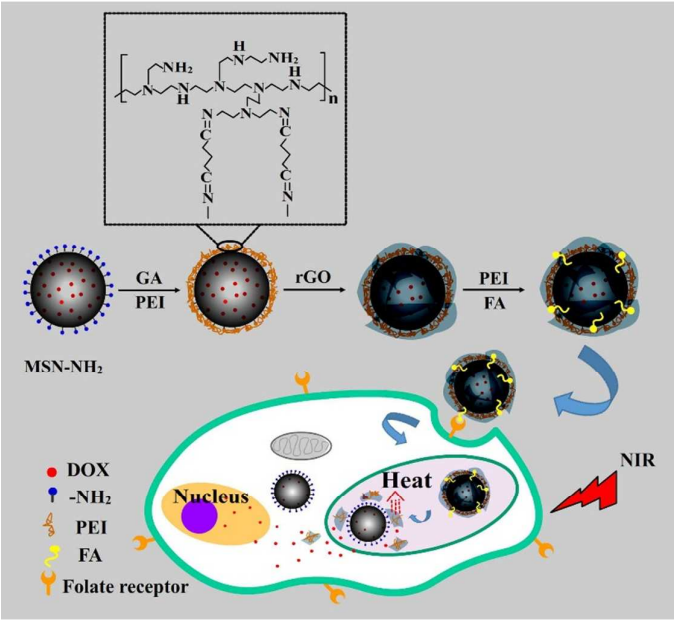

A multifunctional drug delivery system by coupling photothermal therapy and chemotherapy together was developed with high photothermal conversion, low cytotoxicity and high drug loading capacity based on the combination of rGO and MSNs, wherein the cargo molecules could be released in acidic environment due to the well-known pH dependence of cleavage of the C=N bonds of the Schiff' base –bond.